Solid State Ionics 181 (2010) 48–52

Contents lists available at ScienceDirect

Solid State Ionics

journal homepage: www.elsevier.com/locate/ssi

Electrical conductivity of MnO_x–Y_2O_3–ZrO_2 solid solutions

Daria Pomykalska, Mirosław M. Bućko [*], Mieczysław Rękas

AGH, University of Science and Technology, Faculty of Materials Science and Ceramics, al. Mickiewicza 30, 30-059 Krakow, Poland

ARTICLE INFO

Article history:
Received 28 April 2009
Received in revised form 4 November 2009
Accepted 29 November 2009

Keywords:
Zirconia solid solution
MIEC
SOFC

ABSTRACT

Fully stabilized zirconia solid solutions (s.s.) containing manganese seem to be promising materials for intermediate layers between electrolytes and cathodes in solid oxide fuel cells. When manganese is present in zirconia solid solutions, they start to exhibit electronic conductivity due to the formation of some electronic defects related with the variable valence of manganese and, in consequence, activation losses that accompany the transfer of charge between electrolyte and cathode may be reduced. Powders from $Mn_x(Y_{0.148}Zr_{0.852})_{1-x}O_{2-\delta}$ (with x ranging from 0 to 0.25) materials were prepared by means of the co-precipitation–calcination method and then sintered for 2 h at 1500 °C. The compositional dependence of the lattice parameters complied with Vegard's rule up to about 18 mol% of manganese, which confirmed that cubic zirconia s.s. had been formed. The bulk conductivity of the samples and their grain boundaries, determined using impedance spectroscopy, are strictly dependent on their chemical composition. The observed changes in the concentrations of ion and electron defects in cubic zirconia may be utilized in the construction of solid oxide fuel cells.

1. Introduction

Generally, fuel cell efficiency is related with energy losses, which can be divided into three components:

- Ohmic losses, which result from heat production that accompanies the flow of electric current in the internal circuit. They are reduced mainly by decreasing the thickness of the electrolyte. Presently, this thickness has successfully been reduced below 10 µm [1].
- Gas polarization losses, which result from low fluxes of gases feeding the cell (fuel and oxygen).
- Activation losses. Insufficient rates of electrode reactions are the source of this kind of losses. These rates are proportional to the density of three-phase boundaries, *tpb*. The *tpb* involves the points where the solid electrolyte (the source of oxygen ions in the case of an oxygen-conducting electrolyte, or hydrogen ions in the case of a protonic electrolyte), the collector of electrons (electronic conductor, e.g. metal) and the gas phase (source of oxygen or fuel molecules) connect. In the simplest case involving the metal–electrolyte–gas phase boundary, the density of *tpb* is rather low (Fig. 1A). To overcome this obstacle, mixed ionic–electronic conductors, MIECs, are used as electrodes (Fig. 1B). $La_{1-x}Sr_xMO_{3-\delta}$ perovskites, where M = Mn, Co, Fe (and each of these elements may appear alone or in a combination with the others), are used as cathodes [1–3]. These materials show MIEC properties. Ionic conductivity is achieved via the movement of oxygen ions through oxygen vacancies and electronic conductivity occurs as a result of the movement of electron holes [4]. Cermet composites such as YSZ–Ni (where YSZ — yttria-stabilized zirconia) are commonly used as anode materials [5,6]. However, such materials differ considerably in chemical composition and structure from the adjacent solid electrolyte phase. This leads to thermo-mechanical stress and to the heterodiffusion of elements forming these phases. Both phenomena affect the lifetime of the cells negatively.

An alternative solution to the above-mentioned drawbacks is the formation of near-surface layers on an electrolyte exhibiting MIEC behaviour [7]. This goal can be achieved by incorporating transition metals into the surface layers of the electrolyte. The induction of the electronic conductivity component in YSZ was observed when using cerium [8], titanium [9], terbium [10], iron [11], and manganese [12–15] as metal dopants. Manganese appears to be the most promising one among them. The solubility of Mn in YSZ is rather high (above 12 at.% [14]). Solid solutions of YSZ:Mn exhibit mixed ionic–electronic conductivity. The electronic conductivity is the result of the valence change of Mn ions, and occurs via the movement of small polarons. It was also suggested that the addition of Mn yields an improvement of the catalytic efficiency of numerous electrochemical reactions that take place at the electrode–electrolyte interface [16]. Moreover, the presence of a thin layer containing Mn reduces the reactivity between the solid electrolyte and the cathode material, such as LSM, which leads to an increase in the durability of the SOFC [17].

The preparation of MnO_x–Y_2O_3–ZrO_2 solid solutions acting like MIECs is the first stage of the above-described goal, i.e. the reduction of activation losses. It is also the objective realized in this paper, which

---

[*] Corresponding author. Tel.: +48 12 617 3572; fax: +48 12 633 1593.
E-mail address: bucko@agh.edu.pl (M.ŁM. Bućko).

0167-2738/$ – see front matter © 2009 Elsevier B.V. All rights reserved.
doi:10.1016/j.ssi.2009.11.018

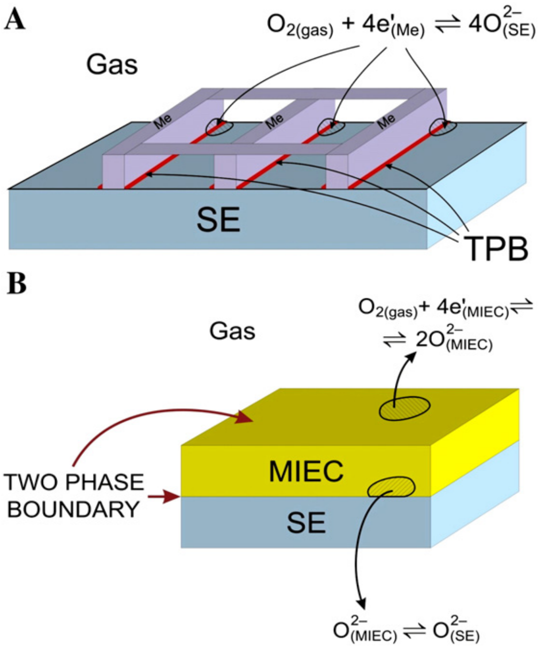

Fig. 1. Schematic illustration: A) three-phase boundary (*tpb*), B) two-phase boundary model.

presents the elaboration of a method for the synthesis of $Mn_x(Y_{0.148}Zr_{0.852})_{1-x}O_{2-\delta}$ solid solutions and the determination of their structural and electrical properties.

2. Experimental

The materials were prepared by means of the co-precipitation–calcination method. Zirconium oxychloride, $ZrOCl_2$ (provided by Merck), yttrium chloride, $YCl_3 \cdot 6H_2O$ (SIGMA-Aldrich) and manganese nitrate, $Mn(NO_3)_2 \cdot xH_2O$ (SIGMA-Aldrich) were used as starting materials. Aqueous solutions of these chemicals were mixed in appropriate proportions. The mixture was then dropped into an extensively stirred solution of NH_3 (1:1). The precipitated gel was washed by means of decantation until Cl^- ions were no longer present (verified with $AgNO_3$). It was then dried at 70 °C for 12 h and calcinated at 700 °C for 1 h. The powders were milled in absolute propanol for 4 h in a rotation-vibrating mill. After that they were pressed in two-steps: uniaxially and then isostatically, under 200 MPa. The obtained pellets were sintered at 1500 °C, for 2 h. The molar ratio of yttrium to zirconium in all solid solutions was fixed as $Y_2O_3:ZrO_2 = 0.08:0.92$, whereas the nominal contents of Mn were: 0; 2.5; 5.0; 10.0; 15.0; 20.0 and 25 mol%.

An X'Pert (Panalytical) XRD diffractometer with monochromatic $CuK_{\alpha 1}$ radiation was used to identify the phase composition and determine the crystallographic parameters of the cell. Based on the experimentally determined half-width of the diffraction reflexes (1 1 1) of the cubic form of ZrO_2 and by applying Scherrer's equation, the size of the crystallites was evaluated. SEM observations (Nova 200 NanoSEM, FEI Company) were performed using samples with polished and thermally etched surfaces.

Impedance spectrometer FRA 1260 and dielectric interface 1294 (both provided by Solartron) were used in the study. The measurements were performed within the 0.1 Hz–1 MHz frequency range at 200–400 °C. Pellets 10 mm in diameter and 2–3 mm thick, with Pt electrodes, were used.

The galvanic cell:

$$\mathrm{Pt}|\ \mathrm{Fe},\ \mathrm{FeO}|\ Mn_x(Y_{0.148}Zr_{0.852})_{1-x}O_{2-\delta}|\mathrm{Ni},\ \mathrm{NiO}\ |\mathrm{Pt} \tag{1}$$

was constructed in order to determine the oxygen transference numbers, t_{ox}, in the studied specimens. The following relationship was used:

$$t_{ox} = \frac{E_e}{E_t} \tag{2}$$

where E_e and E_t denote experimental and theoretical electromotive force, EMF, of the cell, respectively. The theoretical EMF was reported in [18]. The measurements were carried out in the temperature range of 650–950 °C.

3. Results and discussion

XRD analysis revealed that the predominant phase of the samples was the cubic zirconia solid solution. Only for higher concentrations of Mn (20 and 25 mol%), weak reflexes coming from another phase were observed. These reflexes can be attributed to the Mn_2O_3 phase. An increase in Mn content had a considerable effect on crystallite size. The average crystal size was 10 nm of undoped zirconia, while for the sample containing 25 at.% Mn it decreased to 5.2 nm. A similar effect had already been observed for other dopants of ZrO_2 [19].

XRD phase analysis revealed a minor spinel-type Mn_3O_4 phase for the nominal concentrations of 20 and 25 at.% Mn. The meta-stable Mn_3O_4 phase, frozen at room temperature, had been observed earlier by Kim et al. [12]. The estimated contents of Mn_3O_4 in 20 at.% Mn and 25 at.% Mn were 3.6 and 7 wt.%, respectively. Fig. 2 illustrates the value of the cell's crystallographic parameter versus Mn content. The observed linear drop of the parameter within 0–15 at.% Mn may be attributed to the differences between ionic radii of Mn ($r_{Mn2+} = 0.096$ nm; $r_{Mn3+} = 0.058$ nm), Y ($r_{Y3+} = 0.1019$ nm), and Zr ($r_{Zr4+} = 0.084$ nm) [20]. A further increase in Mn content did not cause any changes of the parameter, which was likely due to the fact that by this point the formed solid solutions had become saturated. The solubility limit estimated from Fig. 2 was ca. 18 at.% Mn. This value is higher than the one observed in [12,14]. The cited authors, who used a different method of synthesis (reaction in a solid state) and a different temperature of sintering (1400 °C), reported Mn solubility equal to 12 at.%.

The afore-mentioned presence of the Mn_3O_4 phase detected using the XRD method was confirmed by microscopic observations. Fig. 3 shows the microstructure of the sample containing 25 at.% Mn. Well-developed isometric grains, ca. 10 μm in size, were formed from the saturated solid solution phase. Isolated grains, 3 μm in size, may easily be discerned between them.

Fig. 4 shows the typical impedance spectrum of $Mn_{0.05}(Y_{0.148}Zr_{0.852})_{0.95}O_{2-\delta}$ at 300 °C. Similar plots were obtained in all

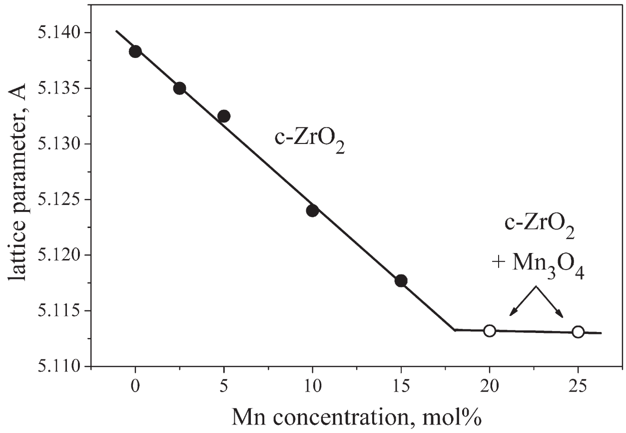

Fig. 2. Compositional dependence of the cell parameter of $Mn_x(Y_{0.148}Zr_{0.852})_{1-x}O_{2-\delta}$.